Large vacuum Rabi splitting in a multiple quantum well GaN-based microcavity in the strong-coupling regime

Gabriel Christmann,[1] Raphaël Butté,[1] Eric Feltin,[1] Anas Mouti,[2] Pierre A. Stadelmann,[2] Antonino Castiglia,[1] Jean-François Carlin,[1] and Nicolas Grandjean[1]

[1]*Institute of Quantum Electronics and Photonics, École Polytechnique Fédérale de Lausanne (EPFL), CH-1015 Lausanne, Switzerland*

[2]*Interdisciplinary Centre for Electron Microscopy, École Polytechnique Fédérale de Lausanne (EPFL), CH-1015 Lausanne, Switzerland*

(Received 29 October 2007; published 14 February 2008)

An AlInN/AlGaN microcavity (MC) containing a GaN/$Al_{0.2}Ga_{0.8}N$ multiple quantum well (MQW) structure is investigated through room temperature (RT) photoluminescence and reflectivity experiments. A vacuum Rabi splitting as large as 50 meV at RT is reported for this MC structure, the highest value reported so far for a semiconductor MC containing QWs. This is shown to result from a geometry combining a state of the art nitride-based MC with a MQW system where the built-in electric field has a reduced impact on the oscillator strength of optical transitions. The contribution of Bragg modes seen in optical spectra is well accounted for by transfer matrix simulations. In addition, the sensitivity of the present system to the tuning between the various optical components of the microcavity (bottom and top Bragg reflectors and active cavity region) to maximize the strong-coupling regime is also shown through simulations. Prospects regarding the nonlinear polariton emission from such a structure indicate that this type of MCs could potentially sustain ultrafast polariton parametric amplification up to 440 K, thanks to an increased exciton binding energy. More generally, it is predicted that, owing to a large exciton saturation density in excess of 1×10^{12} cm^{-2} per QW, such a MC structure would be suitable for the observation of nonlinear effects associated with cavity polaritons (polariton lasing and polariton Bose-Einstein condensates) at RT and above.

DOI: 10.1103/PhysRevB.77.085310 PACS number(s): 78.67.−n, 78.67.De, 71.36.+c, 78.20.Bh

I. INTRODUCTION

Semiconductor microcavities (MCs) operating in the strong light-matter coupling regime (SCR) have generated an intense research effort over the past few years.[1] In this regime, the normal modes are cavity polaritons resulting from the coupling of cavity photons and excitons, which most often gives rise to a new dispersion curve with two branches, the lower polariton branch (LPB) and upper polariton branch (UPB).[1,2] These admixed quasiparticles are composite bosons with a light-matter character varying along the dispersion curve. In particular, polaritons belonging to the bottom part of the LPB are characterized by a strong photonic fraction, i.e., a very small in-plane effective mass compared to excitons (typically 10^4 times lower). As a consequence of such a light mass, the available two-dimensional density of states (2D-DOS) at the bottom of the trap formed by the LPB in k space is relatively small. This reduced 2D-DOS makes this system extremely attractive for reaching polariton state occupancies exceeding unity either under resonant[3–5] or nonresonant excitation,[6–9] thus leading to coherent macroscopic states in the solid state. Among them, Bose-Einstein condensates (BECs) of polaritons have attracted an increasing interest as they occur at temperatures several orders of magnitude higher than in dilute atomic gas systems owing to the light effective mass of polaritons, typically at a few tens of kelvins for the former[7,8] against a few hundreds of nanokelvins for the latter.[10,11] Such polariton BECs, observed so far in a CdTe-based MC[7] and in a GaAs-based MC using a harmonic potential trap,[8] thus open new perspectives regarding the investigation of spontaneous coherence in a system of interacting bosons (this interaction arises due to the Coulomb repulsion issued from the excitonic part of cavity polaritons). However, these results are limited to cryogenic temperatures as experiments were carried out at $T=4-5$ K leading to an effective carrier temperature of ~100 K at most.[8]

In this context, the recent report of room temperature (RT) polariton lasing in a bulk GaN MC[9] appears as a very promising step toward the in-depth study of coherent polariton phases at cryogenic temperatures and above as well as for the future realization of functional low-threshold polariton laser devices. This is made possible thanks to the large exciton binding energy (E_X^B) and large coupling of excitons to the light field, an inherent characteristic of wide band gap III-nitride epilayers.[12]

Early studies carried out on strongly coupled nitride-based MCs primarily focused on bulk GaN cavities[13,14] due to their simpler geometry and the improved optical properties of bulk GaN layers over nitride-based quantum wells (QWs). Indeed, the former exhibit a reduced inhomogeneous broadening, an aspect of crucial importance as such broadening can possibly prevent the system reaching the SCR. Besides, it allows getting rid of the quantum confined Stark effect (QCSE) resulting from the built-in electric field (F_{bi}) inherent to III-nitride heterostructures grown along the c axis.[15,16] However, the physics of bulk GaN MCs differs somewhat from that of planar QW-MCs as in such a bulk GaN structure up to three bulk [three-dimensional (3D)] excitons can couple to 2D-cavity photons leading to the formation of 2D-cavity polaritons.[14] Besides, the exciton binding energy of bulk GaN excitons is about 25–27 meV,[17] a value not markedly larger than that of excitons in CdTe-based QW-MCs.[6] Finally, with the aim of realizing an electrically pumped polariton laser, a more realistic structure would use

QWs embedded in a *p-n* junction as such a geometry ensures an improved confinement of the carriers leading to a lower threshold.

Consequently, it appeared natural to implement a nitride-based QW-MC as both the exciton oscillator strength (f_{osc}) and E_X^B are expected to be larger in such a system. Note, however, that in III-nitride heterostructures grown along the *c* axis, this is indeed the case provided that the QW thickness is not too large to ensure a maximum overlap of the electron and hole wave functions, i.e., to minimize the impact of the QCSE.[15,16] With this constraint in mind, a hybrid $3\lambda/2$ AlInN/AlGaN MC containing two sets of three narrow GaN/AlGaN QWs [5 ML (monolayer) thick] was grown[18,19] using a design directly inspired from standard planar QW-MCs made of III-V arsenides.[3] The use of GaN/AlGaN QWs rather than InGaN/GaN ones is justified by their lower inhomogeneous broadening (see also discussion below).[18] A vacuum Rabi splitting (Ω_{VRS}) of 30 meV was measured at RT for this structure from which an f_{osc} of 4.8×10^{13} cm^{-2} per QW was inferred, a value 1 order of magnitude larger than for InGaAs/GaAs QWs.[18] However, despite this large Ω_{VRS} value slightly in excess of k_BT at RT, the line shape of corresponding photoluminescence (PL) spectra was shown to be inhomogeneously broadened from an analysis based on a linear dispersion model.[18] It was first assumed that this inhomogeneous PL linewidth was essentially of excitonic origin, a usual assumption made for planar QW-MCs.[20] However, later studies performed on equivalent crack-free empty AlInN-based MCs revealed that the cavity mode is also strongly inhomogeneously broadened at the scale of laser spot sizes typical of PL experiments ($\sim$50 μm in diameter) mainly due to in-plane disorder occurring in the cavity layer and in the distributed Bragg reflectors (DBRs).[21]

A possible way to overcome or at least reduce the impact of inhomogeneous broadening consists in increasing the number of QWs (N_{QW}) inserted in the cavity region.[20] Indeed, Ω_{VRS} is known to scale with N_{QW},[22] namely, $\Omega_{VRS} \propto \sqrt{N_{QW}}$, provided that these QWs are efficiently coupled to the cavity light field, i.e., if the wells are located at an antinode of the electromagnetic field propagating in the cavity. As a consequence, this should also help increasing the Ω_{VRS} to polariton linewidth ratio at the resonance, a well-known figure of merit to assess the quality of the SCR in semiconductor MCs.

Following this preliminary analysis, we report in this paper a thorough study of a crack-free hybrid AlInN/AlGaN microcavity containing a GaN/AlGaN MQW active region. First, a sample description and experimental details are given. Then, an optical characterization of the MQWs is carried out on the half-MC structure. The full MC structure is then characterized by means of RT PL and reflectivity (*R*) measurements revealing a vacuum field Rabi splitting of 50 meV, the highest value reported so far for a QW-based microcavity structure. The interplay between the different building blocks of the structure (bottom and top DBRs, MQW active region) and their implication on the experimental observations are then discussed via a proper modelization based on a transfer matrix model. Finally, some tentative predictions regarding the adequation of such a MQW-MC structure for nonlinear polariton emission studies are also made.

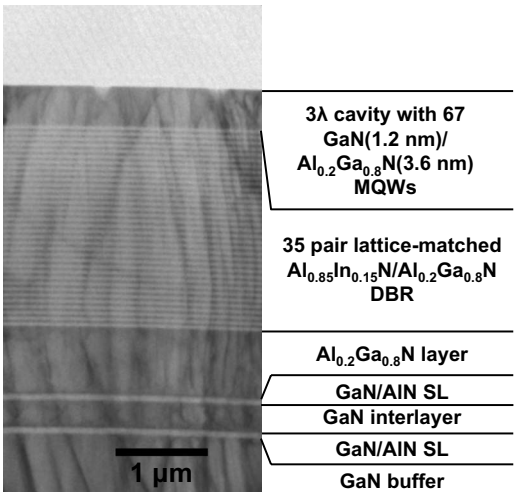

FIG. 1. Cross-section transmission electron micrograph of the half-microcavity structure.

II. SAMPLE DESCRIPTION AND EXPERIMENTAL DETAILS

The present MQW-MC structure was grown by metal-organic vapor phase epitaxy (MOVPE) on a standard 3 μm thick GaN buffer layer on *c*-plane sapphire substrate. It then consists of a strain relieving template, followed by an $Al_{0.2}Ga_{0.8}N$ layer on which a 35 pair lattice-matched $Al_{0.85}In_{0.15}N/Al_{0.2}Ga_{0.8}N$ DBR is grown. Growth details on such AlInN-based DBRs have been reported elsewhere.[23] The cavity layer has a 3λ optical thickness and is made of a $5\lambda/2$ active region consisting of a 67 period GaN(1.2 nm)/$Al_{0.2}Ga_{0.8}N$(3.6 nm) MQW structure sandwiched between two $\lambda/4$ $Al_{0.2}Ga_{0.8}N$ layers. The structure was finally completed by a 13 pair SiO_2/Si_3N_4 DBR grown *ex situ* by plasma enhanced chemical vapor deposition. Such a geometry allows an efficient stress management leading to an entirely crack-free structure, as checked by phase contrast optical microscopy. A cross-section transmission electron microscopy image of the half-microcavity structure (i.e., prior to the deposition of the dielectric DBR) is shown in Fig. 1.

RT angular-resolved reflectivity measurements were performed by means of a two arm goniometer in θ-θ configuration. A xenon lamp was employed as a white light source. The incoming light beam was brought by a 100 μm core optical fiber and imaged onto the sample with a 3:4 magnification. The reflected light was then collected by a 400 μm core UV optical fiber using appropriate optics offering an angular selection of $\pm1°$ and detected by a liquid nitrogen cooled UV-enhanced charge-coupled device monochromator combination. The reflectivity spectrum from an aluminum mirror was taken as a reference. To perform reflectivity measurements under normal incidence, a beam splitter was placed on the light path. RT angular-resolved PL measurements were performed under weak excitation power (50–100 W cm^{-2}) using the 244 nm line of a continuous

wave Ar^+ laser frequency-doubling unit. The laser beam was focused down to a 50 μm diameter spot on the top dielectric DBR and incident at a fixed angle. The emitted light was then collected using the same collection unit as in R measurements. Microphotoluminescence (μPL) measurements have also been performed by focusing the laser beam using a long working distance UV microscope objective ($80\times$) with a numerical aperture of 0.55 (laser spot size <1 μm). The light emitted along the normal to the sample was collected by a 400 μm core UV optical fiber in far field configuration, ensuring an angular selection of 0.6°.

III. EXPERIMENTAL RESULTS AND DISCUSSION

A. Geometry and analysis of the multiple quantum well system

As mentioned in the Introduction, the use of a large number of QWs should allow increasing significantly Ω_{VRS}. The motivation for choosing a MQW system such as that described in the previous section is essentially twofold. First, it greatly simplifies the growth as no specific care has to be taken to ensure that the wells are exactly positioned at a cavity light field antinode, as these are uniformly distributed across the cavity region. Besides, the wells will all undergo the same F_{bi} owing to the geometrical effect,[24,25] which is not the case for the sets of three wells used in the previous nitride-based QW-MC structure (due to varying barrier thicknesses).[18] As a consequence, the impact of the electric field on the inhomogeneous broadening should be smaller due to its uniformity across the structure. Indeed, due to the QCSE, wells experiencing different values of F_{bi} should emit at different wavelengths.[16] Note that the width of the wells was intentionally kept narrow ($\sim$5 ML thick) as such QWs have been shown to be the best compromise in terms of PL linewidth and oscillator strength.[18,19]

It is worth pointing out that, owing to the heavy mass of carriers in nitrides,[26] adjacent wells separated by such a barrier thickness (3.6 nm) will not couple together to form minibands, as it is usually the case in equivalent III-V arsenide MQWs.[27] In this respect, it is worth pointing out that MCs with an embedded GaAs/AlGaAs superlattice (SL) operating in the SCR up to RT have already been reported.[28] However, in this latter case, Ω_{VRS} was limited to 8.5 meV.

The two $\lambda/4$ $Al_{0.2}Ga_{0.8}N$ spacers surrounding the active MQW region are introduced both for symmetry reason as well as to ensure optimum growth conditions for the MQWs. Indeed, the thicker the $Al_{0.2}Ga_{0.8}N$ *template* will be, the better the quality of these narrow wells. In other words, GaN QWs grown directly on top of the bottom $Al_{0.85}In_{0.15}N/Al_{0.2}Ga_{0.8}N$ DBR would exhibit a much worse optical quality likely due to an increased interface roughness.[29]

A consequence of the present geometry, not explicitly mentioned so far, is that all the wells will not be efficiently coupled to the cavity light field.[22] As shown in previous theoretical treatments of strongly coupled MCs,[30,31] excitonic states are rearranged through radiative coupling into a single *bright* state for which the coupling to the light field is maximal and *dark* states exhibiting almost no coupling to the light field. Overall, the effective number of wells N_{eff} coupled to the light field will be smaller than N_{QW} leading to a value of Ω_{VRS} scaling less than $\sqrt{N_{QW}}$. However, the gain induced by the use of such a geometry in terms of Ω_{VRS} over previous QW-MC structures with the QWs inserted at the cavity light field antinodes will be demonstrated hereafter.

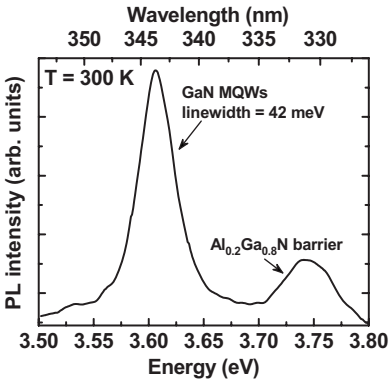

FIG. 2. RT PL spectra of the 67 period $GaN/Al_{0.2}Ga_{0.8}N$ MQW structure.

As quoted above, for a structure with a small number of wells per antinode, the side wells do not experience the same F_{bi}, which leads to an inhomogeneous broadening of the QW emission. In the present geometry, the side QWs should have a lower contribution compared to the other wells. In addition, they are positioned at a cavity light field node so that their impact should be nearly negligible.

To assess the quality of the present 67 period MQW system, RT PL measurements have been performed on the half-cavity structure. The PL linewidth is about 42 meV at RT, which establishes the state of the art for such heterostructures (Fig. 2). Note that such a value compares well with that of MOVPE grown GaN epilayers measured at RT[32] and that of previous bulk half-cavity structure.[14]

Another parameter to be properly taken into account when analyzing the full MC structure is the effective value of the refractive index for the cavity region. Indeed, in addition to the excitonic resonance, the real part of the complex refractive index of the wells will have to be considered as the latter will affect values such as the penetration length into the DBRs.

B. Angle-resolved measurements

The optical quality of the complete MQW-MC structure was first assessed by performing μPL measurements on a region exhibiting a large negative detuning $\Delta(=\omega_{cav}-\omega_X)$ between cavity photons of pulsation ω_{cav} at zero in-plane wave vector $k_{\|}$ and excitons of pulsation ω_X in order to probe the intrinsic properties of the cavity photon mode. A typical RT μPL spectrum for such a region is shown in Fig. 3(a), from which a quality factor $Q(=\lambda/\Delta\lambda)=1040$ is extracted. Such a value emphasizes the high local quality of our MC structures, which corresponds to the state of the art for a nitride-based QW-MC.[34] However, its is known that on a larger scale, an important in-plane cavity disorder is present, as revealed by μ-transmission mappings.[21] As a result, when

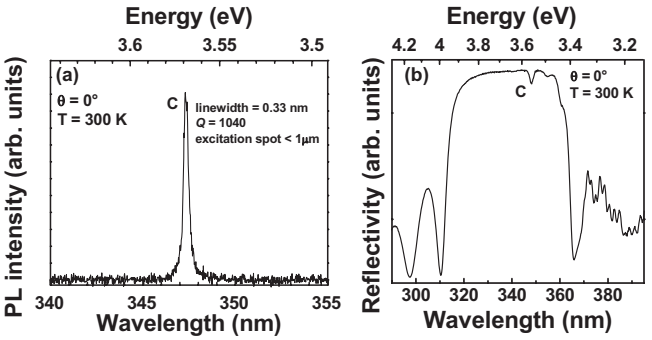

FIG. 3. (a) RT normal incidence μPL spectrum of the complete MQW-MC structure in a cavitylike region. (b) RT normal incidence reflectivity spectrum of the complete MQW-MC structure.

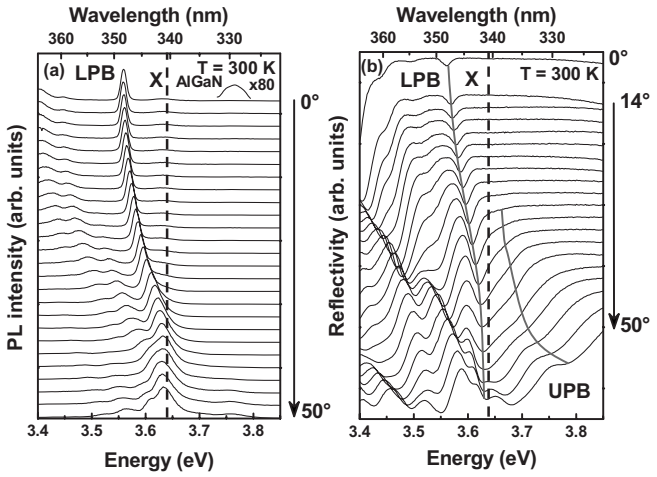

FIG. 4. (a) RT angle-resolved PL spectra ranging from 0 to 50°, measured every 2° and downshifted for clarity. (b) RT angle-resolved reflectivity spectra ranging from 0 to 50°, measured every 2° (except at small angles) and downshifted for clarity. The dashed line corresponds to the uncoupled QW exciton energy. Gray lines are a guide for the eyes, showing the dispersion of polariton branches.

performing standard reflectivity or PL measurements, the contribution of different cavities emitting at different wavelengths is likely to be probed. As an illustration of the inhomogeneous broadening of the cavity mode probed when using a larger spot size, a RT normal incidence reflectivity spectrum of the complete MQW-MC structure is reported in Fig. 3(b). The spectrum exhibits a flat-topped stop band about 50 nm wide with the cavitylike mode (C) (actually the photonlike LPB, as will be shown hereafter) slightly redshifted compared to the center of the stopband arising mainly from the dielectric DBR. A Q factor $\sim$200 is extracted from this spectrum, a value significantly lower (by a factor of 5) than that measured with the μPL setup. The small dip next to C corresponds to the low energy end of the bottom $Al_{0.85}In_{0.15}N/Al_{0.2}Ga_{0.8}N$ DBR stop band. The sidelobes on the low energy side of the spectrum are characterized by a complex structure arising from the modulation between the two DBRs having layers of different nature (and thus different refractive indices). On the other hand, the high energy side exhibits a more regular pattern issued from the top dielectric DBR only as the incoming probe light is absorbed by the AlGaN cavity.

RT angle-resolved PL spectra measured on a wide range of angles (taken every 2° up to 50°) are reported in Fig. 4(a). A parabolic dependence for the LPB dispersion is observed at small angles in the PL spectra followed by an asymptotic trend toward the uncoupled exciton energy (X) [Fig. 4(a)]. No signature of the upper polariton branch is visible on this graph plotted in linear scale. This is a common feature of wide band gap MCs, which is usually ascribed to the combined influence of PL thermalization effects, as already reported for II-VI MCs[6] and possible intracavity absorption.[14,18] We can also notice the presence at small angles of a nondispersive PL peak at the exciton energy associated with dark states[30] as well as the weak luminescence of the $Al_{0.2}Ga_{0.8}N$ barriers occurring at $\sim$3.75–3.77 eV. Note also that the spectral shape of the LPB is strongly modified when increasing the collection angle. This results from the fact that beyond a certain critical angle (here $\theta_c \sim 34°$), MQW excitons will radiate out of the DBR stop band. In the present case, polaritons are not confined anymore by the top dielectric DBR which has a much steeper stop band dispersion, owing to the reduced refractive index of its bilayer constituents compared to the bottom nitride one.[33] Such a phenomenon has been already pointed out to occur for such wide band gap MC structures.[34] Besides, in a system such as the present one where the exciton oscillator strength is large, coupling of MQW excitons to Bragg modes (BMs), i.e., leaky modes, is likely to occur.[9,35] Such coupling will be addressed further below.

Complementary information on this MQW-MC structure can be gained by studying the evolution of RT R spectra vs angle. Such a series of spectra is reported in Fig. 4(b) for angles up to 50°. A clear correspondence is observed between this measurement set and the PL one for the LPB. However, contrary to PL measurements, an additional dip exhibiting a clear dispersion is observed at high angles above the uncoupled exciton energy. This is the signature of the upper polariton branch.[36] In addition, at even higher angles, we observe the appearance of an additional reflectivity dip located between the polariton branches. As mentioned for the angle-resolved PL spectra, this is the contribution of a Bragg mode to the SCR. The signature of other BMs, which will be properly labeled and analyzed in the next subsection, is also visible below the LPB.

C. Modeling of experimental reflectivity results

To get a better understanding of the underlying physics issued from R spectra and, in particular, to determine the impact of BMs, simulations have been carried out in the framework of the transfer matrix theory.[33] The refractive indices for nitride compounds are taken from the work of Brunner *et al.*[37] (AlGaN alloys) and Carlin *et al.*[38,39] (AlInN alloys). The optical properties of SiO_2 and Si_3N_4 layers were determined using thick layers grown on sapphire substrates. The quantum wells are modeled by a Lorentz oscillator dispersive dielectric function $\epsilon(\omega)$. For the sake of clarity, we

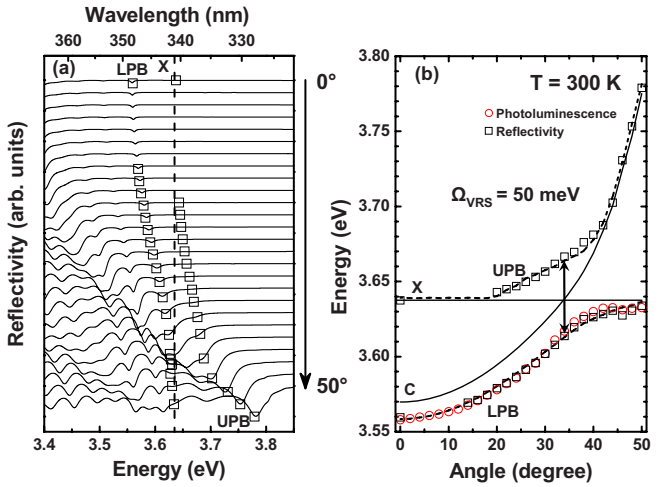

FIG. 5. (Color online) (a) Computed angle-resolved reflectivity spectra ranging from 0 to 50°, calculated every 2° and downshifted for clarity. Empty squares correspond to the experimental RT reflectivity minima ascribed to the LPB and the UPB. (b) RT experimental dispersion curves deduced from reflectivity spectra (empty squares) and PL spectra (empty red circles) and fits of the LPB and the UPB (dashed lines). The cavity mode (C) and the uncoupled exciton (X) are also reported (black lines).

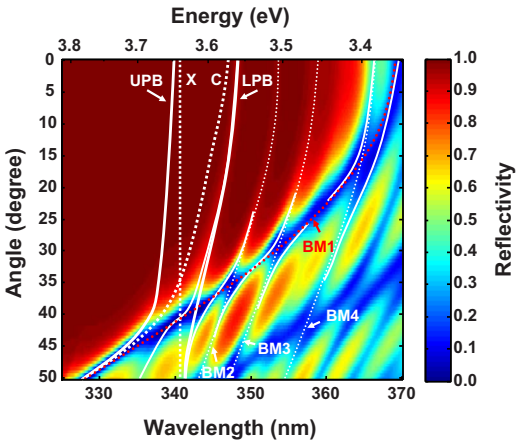

FIG. 6. (Color online) Color map of the computed angle-resolved reflectivity spectra ranging from 0 to 50° for wavelengths ranging between 325 and 370 nm. Various branches are reported, namely, the polariton branches (LPB and UPB, thick white lines), the uncoupled exciton and the cavity modes (X and C, dashed white lines), the first Bragg mode of the dielectric DBR (BM1, dotted red line), the Bragg modes of the bottom nitride DBR (BM2-4, dotted white lines), and the coupled Bragg modes (thin white lines).

did not include the contribution of the inhomogeneous broadening when computing the spectra, as the main aim of this section is to reproduce the dispersion curve of the various modes observed in the experimental spectra (i.e., LPB, UPB, and BMs) rather than their exact spectral shape. Note that provided that sources of broadening are smaller than Ω_{VRS}, which is indeed the case here, such an analysis is *a priori* justified as the dispersion curves should not be significantly modified.[18]

Computed reflectivity spectra ranging from 0 to 50° with a 2° step are shown in Fig. 5(a) together with experimental data points for the LPB and the UPB (black squares). An excellent agreement is found between experiment and theory when using the nominal thicknesses and a value of f_{osc} of 5.1×10^{13} cm^{-2} to describe each QW. Note that this latter value exceeds slightly (by ~6%) that previously determined for a nitride MC containing six GaN/$Al_{0.2}Ga_{0.8}N$ QWs[18] of equivalent thickness but for which the built-in electric field is likely larger due to a different geometry.[24,25] It is worth pointing out that the signature of the UPB is hardly seen even at the anticrossing point, as observed in R experiments. As will be confirmed hereafter, this results from the blue-shifted position of the top dielectric DBR with respect to the bottom nitride DBR and the cavity region. The RT experimental and theoretical polariton dispersion curves (LPB and UPB) as well as the uncoupled modes (X and C) are reported in Fig. 5(b). A RT vacuum Rabi splitting of 50 meV is extracted from this plot, the highest value reported so far for a QW-based MC structure.

A color map of the angular dispersion of computed R spectra in the wavelength range 325–370 nm is shown in Fig. 6. Polariton branches (thick white lines) and the uncoupled exciton mode and the cavity mode (dashed lines) are marked together with Bragg modes (dotted lines) from the low energy side of the stop band. As expected, the Bragg mode associated with the dielectric DBR (BM1, dotted red line) exhibits the steepest dispersion owing to its reduced effective refractive index. It is also seen that BM1 crosses all the other modes. On the other hand, BMs associated with the nitride DBR (BM2-BM4, dotted white lines) exhibit a much lower dispersion. These Bragg modes also exhibit a complex behavior, as they appear to be all coupled with BM1 or with the polariton branches (thin white lines), as previously reported for a bulk nitride MC.[9] The interplay between these photonic modes leads to anticrossings of splitting Ω_{BM_i} ~15–25 meV. Note that such coupling between photonic modes has been previously reported for chains of coupled micron sized semiconductor cavities.[40]

It is worth mentioning that the experimental Ω_{VRS} to polariton linewidth ratio is not as good as could have been expected from such a structure [cf. Fig. 4(b)]. As implicitly suggested above, this is explained by the fact that at large angles, polariton modes are not optimally confined by the DBRs. Anticrossing between polariton modes is, however, observed, thanks to the large oscillator strength of excitons in this MQW system. In the present configuration, the angle where anticrossing occurs (θ_{VRS}) is thus seen to be about equal to θ_c.[41] Such a situation is frequently reported for organic-based MCs operating in the SCR,[42] as the latter are also characterized by large Ω_{VRS} values (which can well exceed that reported in the present work). In order to improve this ratio, an optimal tuning between the optical components of the microcavity (bottom and top DBRs and GaN/$Al_{0.2}Ga_{0.8}N$ MQW cavity) and QW excitons is thus required. In particular, to increase noticeably θ_c, the uncoupled exciton mode should be positioned on the high energy side of the dielectric DBR stop band. At the same time, the cavity mode—whose position is essentially fixed by the DBR central wavelength owing to the penetration depth of

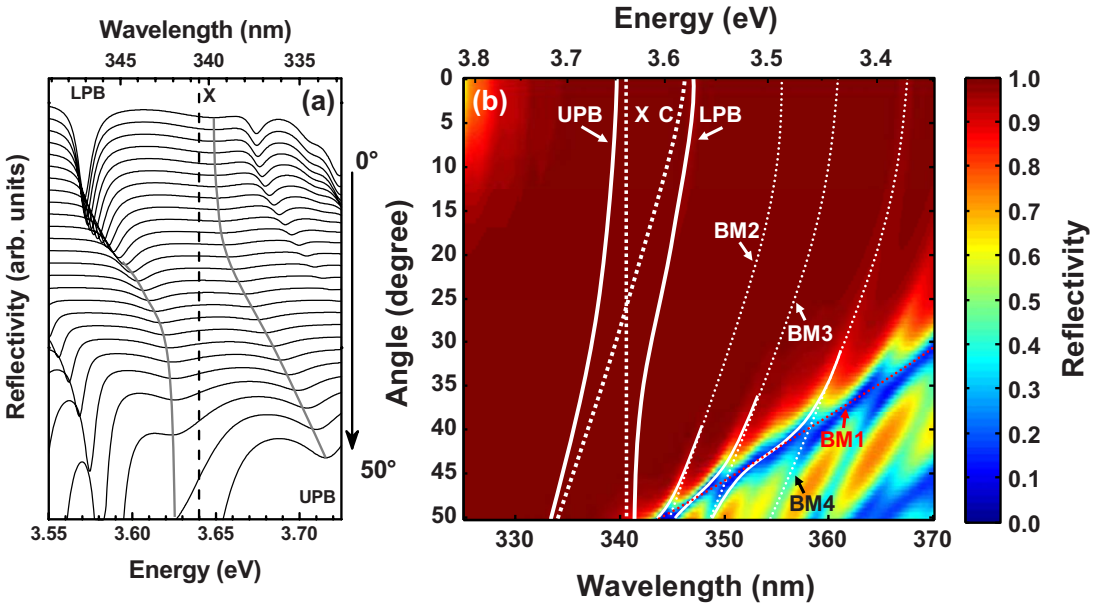

FIG. 7. (Color online) (a) Computed angle-resolved reflectivity spectra ranging from 0 to 50°, calculated every 2° and downshifted for clarity, of the MQW-MC with the top dielectric DBR redshifted by 6%. The dashed line corresponds to the uncoupled QW exciton energy. Gray lines are a guide for the eyes, showing the dispersion of polariton branches. (b) Color map of the computed angle-resolved reflectivity spectra ranging from 0 to 50° for wavelengths ranging between 325 and 370 nm of the MQW-MC with the top dielectric DBR redshifted by 6%. Various branches are reported, namely, the polariton branches (LPB and UPB, thick white lines), the uncoupled exciton and the cavity modes (*X* and *C*, dashed white lines), the first Bragg mode of the dielectric DBR (BM1, dotted red line), the Bragg modes of the bottom nitride DBR (BM2-4, dotted white lines), and the coupled Bragg modes (thin white lines).

the EM field into the DBRs[31]—should also be located on the high energy side of the dielectric DBR stop band, see Figs. 7(a) and 7(b) hereafter, for the anticrossing to occur within the stop band for Δ values <0.[43] Within this scheme, the choice of the central wavelength of each DBR shall depend on their respective stop band angular dispersion. In such a situation, where narrower polariton modes are expected due to an improved optical confinement over the previous situation, an increase of Ω_{VRS} should also be observed as this latter quantity is known to depend on the cavity mode linewidth when such a value is comparable to the intrinsic coupling strength V between cavity photons and QW excitons (for vanishingly small values of the exciton and cavity mode linewidths, Ω_{VRS} reduces to $\Omega_{VRS}=2V$).[22,44] It is worth noting that this last remark is independent of the inhomogeneous broadening of the cavity mode since it is a matter of pure optical confinement which is considered.

As an illustration of the increase of Ω_{VRS} and θ_c when modifying the tuning of the DBRs, simulations of *R* spectra ranging from 0° to 50° for the present MQW-MC structure with the top dielectric DBR redshifted by 6% ($\Delta\lambda \sim 20$ nm) with respect to the current experimental situation, while all other physical parameters are left otherwise unchanged, are shown in Figs. 7(a) and 7(b). Ω_{VRS} and θ_c increase up to 56 meV [Fig. 7(a)] and $\sim 46° - 50°$ [Fig. 7(b)], respectively. In addition, it is seen that the signature of the UPB at the anticrossing is as well resolved as that of the LPB compared to the previous case (here, the anticrossing occurs at $\theta_{VRS} \sim 26°$), thereby showing the high sensitivity of *R* spectra on the fine tuning of the MC optical components. This sensitivity of *R* spectra (also applicable to PL ones) well exceeds that of GaAs-based MCs due to the lower Ω_{VRS} values measured in this latter system compared to the MC stop band width and the reduced angular dispersion of polariton branches owing to the larger average refractive index of the cavity. The increase of θ_c ($\Delta\theta_c \geq 10°$ between the two geometries) thus implies a better optical confinement of the LPB and the UPB within the stop band in the usual range of angles probed in angle-resolved experiments. In other words, it illustrates the reduced impact of BMs on the standard two polariton branches characteristic of the SCR in optimized MC structures characterized by large Ω_{VRS} values.

D. Prospects on the nonlinear polariton emission from nitride-based multiple quantum well microcavities

It is beyond the scope of this paper to investigate the nonlinear optical properties of such a MQW-MC in the polariton regime. However, this is of current practical interest to determine whether the latter type of structure would be suitable for the observation of high-temperature ultrafast polariton parametric amplification (PPA),[4] RT polariton lasing as it was recently the case for a bulk nitride MC,[9] or even polariton BEC. In other words, can such a MC structure be used to go beyond standard linear optical properties of strongly coupled MCs?

Parameters of interest to establish a figure of merit of such a MQW-MC are the exciton binding energy (E_X^B) and the exciton saturation density (n_X^{sat}). E_X^B has been calculated using the variational approach developed by Leavitt and Little,[45] which fully takes into account the impact of F_{bi}. Such a

method was already successfully applied to determine E_X^B in similar GaN/AlGaN QWs.[46] When considering geometrical effects, F_{bi} is found to range between 790 and 1075 kV/cm in the present MQW structure. The lower limit is deduced from the experimental measurements of Ref. 46, while the upper one is deduced from calculations including the piezoelectric polarization and the nonlinear dependence of the spontaneous polarization discontinuity with varying aluminum content.[47] Using these values of F_{bi}, the derived value of E_X^B ranges between 47 and 49 meV, whereas in the absence of any electric field (i.e., under flatband conditions), E_X^B would be equal to 52 meV. It is thus seen that the change of F_{bi} induces only a minor change of the E_X^B value for a system with such narrow wells. Note, however, that the validity of these values is genuinely restricted to the low power density regime, i.e., to excitation conditions where no screening of F_{bi} occurs. In the opposite case, E_X^B is predicted to first increase with increasing exciton density (n_X) before collapsing when n_X gets closer to n_X^{sat}.[48] Using such values of E_X^B would lead to a cutoff temperature ranging between 415 and 440 K, assuming that the linear dependence given in Ref. 4 for the gain as a function of the exciton binding energy in the PPA process would also hold for the present nitride-based MQW-MC structure. This is about 200 K more than the highest cutoff temperature ever reported for such a nonlinear process (220 K in a CdTe-based QW-MC),[4] making nitride MQW-MCs very promising for the realization of nonlinear devices.

In order to obtain a rough estimate of n_X^{sat}, we need to determine the effective Bohr radius (a_B^{eff}) of excitons in our MQW system. A simple approach consists in using the analytic expressions issued from the model developed by He[49] that considers the fractional dimensionality α of a given excitonic system (with $1<\alpha<3$). Thus, for the fundamental ($n=1$) excitonic transition, we get the relationship

$$E_X^B = \frac{\mathrm{Ry}^*}{\left(1+\frac{\alpha-3}{2}\right)^2}, \tag{1}$$

where Ry^* is the bulk exciton Rydberg ~25 meV for X_A and X_B excitons.[17] The fractional dimensionality experienced by the confined excitons is thus given by

$$\alpha = 1 + 2\sqrt{\frac{\mathrm{Ry}^*}{E_X^B}}. \tag{2}$$

From the above-mentioned values of E_X^B in the presence of a built-in electric field, we obtain $\alpha=2.43-2.46$. Note here that the model of fractional dimensionality is assumed to be valid as the impact of the QCSE is negligible in such thin QWs (as can be seen from the minor change in E_X^B between the flatband conditions and our experimental situation). a_B^{eff} for the fundamental excitonic state is then given by

$$a_B^{eff} = a_B^{3D}\left[1+\frac{\alpha-3}{2}\right]^2, \tag{3}$$

where a_B^{3D} is the bulk exciton Bohr radius given by $a_B^{3D}=(\epsilon_r m_0/\mu)a_0$, a_0 is the hydrogen Bohr radius, ϵ_r is the relative dielectric constant of GaN ($\epsilon_r=10.28$),[50] m_0 is the free electron mass, and μ is the exciton reduced mass $1/\mu=1/m_e^*+1/m_h^*$ with $m_e^*=0.20m_0$ and $m_h^*=1.10m_0$ the electron and hole effective masses, respectively.[51] This leads to $a_B^{eff}\sim 1.64-1.71$ nm.

To determine n_X^{sat}, we then make use of the well-known theory developed by Schmitt-Rink *et al.*[52] describing the saturation of the excitonic absorption in a QW system.[53] The exciton saturation density is thus given by $n_X^{sat}\pi(a_B^{eff})^2 \sim 0.117$, an expression which was shown to be valid whatever the effective dimensionality of the QW system of interest.[52] This leads in our case to $n_X^{sat}\sim(1.27-1.38)\times 10^{12}$ cm^{-2}, i.e., a saturation density per QW more than 1 order of magnitude larger than those reported for InGaAs-based QW-MCs[54,55] (18–32 times larger) and about 2.7 larger than in CdTe-based QW-MCs.[6] Using the simplified picture, often considered when treating MCs,[55] assuming that excitons are uniformly created across the structure, it would lead to an exciton sheet density at saturation about $(8.5-9.2)\times 10^{13}$ cm^{-2} when considering all the QWs.

Owing to the reduced density of states accessible to cavity polaritons at the bottom of the LPB,[5] such large values of n_X^{sat} appear indeed very promising regarding the observation of nonlinear effects associated with cavity polaritons for carrier densities well below the saturation limit (both for resonant and nonresonant excitation conditions). This should be effectively the case provided that carrier relaxation is efficient in such system (nonresonant excitation case), which is indeed the case in bulk GaN MCs.[9] It thus opens interesting perspectives for the practical realization of polariton devices operating at RT and above.

Finally, note also that it would be of interest to investigate such QW-MC structures grown along nonpolar orientations, as it would allow getting rid of the QCSE while having f_{osc} values superior to the bulk case. Besides, for such orientations, it would also be possible to grow thick wells (i.e., $\gg a_B^{eff}$) for which the impact of interface roughness will be smaller, thereby reducing further their inhomogeneous broadening.

IV. CONCLUSION

In conclusion, we have shown that a nitride-based MC containing a 67 period $GaN/Al_{0.2}Ga_{0.8}N$ MQW structure exhibits a vacuum Rabi splitting as large as 50 meV at RT, the highest value reported so far for a semiconductor MC containing QWs. This results from an advantageous geometry combining a state of the art nitride-based MC with a MQW system where the built-in electric field has a reduced impact on the oscillator strength of optical transitions. The contribution of Bragg modes seen in optical spectra (both in photoluminescence and reflectivity spectra) is well accounted for by transfer matrix simulations. In addition, the sensitivity of the present system to the tuning between the optical components of the microcavity (bottom and top DBRs and active

cavity region) to maximize the strong-coupling regime has been emphasized through simulations. It has thus been shown that nearly optimized nitride-based MQW-MCs should exhibit even larger Ω_{VRS} and θ_c values and thus a better optical confinement of the LPB and the UPB within the stop band. Prospects regarding the nonlinear polariton emission from such a structure indicate that these MCs could potentially sustain ultrafast polariton parametric amplification up to 440 K, thanks to an increased exciton binding energy. More generally, it is predicted that the observation of nonlinear effects associated with cavity polaritons (polariton lasing and polariton BEC) at RT and above in such a structure is likely owing to a large exciton saturation density in excess of 1×10^{12} cm^{-2} per QW.

ACKNOWLEDGMENTS

This work was supported by the EU FET-Open Program, Stimscat FP6-517769, by the NCCR Quantum Photonics (NCCR QP), research instrument of the Swiss National Science Foundation (SNSF), and by the FNS 200020–113542. N.G. and R.B. are indebted to the Sandoz Family Foundation for its financial support.

[1] For reviews, see, e.g., M. S. Skolnick, T. A. Fisher, and D. M. Whittaker, Semicond. Sci. Technol. **13**, 645 (1998); J. Keeling, F. M. Marchetti, M. H. Szymańska, and P. B. Littlewood, *ibid.* **22**, R1 (2007).

[2] C. Weisbuch, M. Nishioka, A. Ishikawa, and Y. Arakawa, Phys. Rev. Lett. **69**, 3314 (1992).

[3] P. G. Savvidis, J. J. Baumberg, R. M. Stevenson, M. S. Skolnick, D. M. Whittaker, and J. S. Roberts, Phys. Rev. Lett. **84**, 1547 (2000).

[4] M. Saba, C. Ciuti, J. Bloch, V. Thierry-Mieg, R. André, Le Si Dang, S. Kundermann, A. Mura, G. Bongiovanni, J. L. Staehli, and B. Deveaud, Nature (London) **414**, 731 (2001).

[5] R. M. Stevenson, V. N. Astratov, M. S. Skolnick, D. M. Whittaker, M. Emam-Ismail, A. I. Tartakovskii, P. G. Savvidis, J. J. Baumberg, and J. S. Roberts, Phys. Rev. Lett. **85**, 3680 (2000).

[6] Le Si Dang, D. Heger, R. André, F. Boeuf, and R. Romestain, Phys. Rev. Lett. **81**, 3920 (1998).

[7] J. Kasprzak, M. Richard, S. Kundermann, A. Baas, P. Jeambrun, J. M. J. Keeling, F. M. Marchetti, M. H. Szymańska, R. André, J. L. Staehli, V. Savona, P. B. Littlewood, B. Deveaud, and Le Si Dang, Nature (London) **443**, 409 (2006).

[8] R. Balili, V. Hartwell, D. Snoke, L. Pfeiffer, and K. West, Science **316**, 1007 (2007).

[9] S. Christopoulos, G. Baldassarri Höger von Högersthal, A. Grundy, P. G. Lagoudakis, A. V. Kavokin, J. J. Baumberg, G. Christmann, R. Butté, E. Feltin, J.-F. Carlin, and N. Grandjean, Phys. Rev. Lett. **98**, 126405 (2007).

[10] M. H. Anderson, J. R. Ensher, M. R. Matthews, C. E. Wieman, and E. A. Cornell, Science **269**, 198 (1995).

[11] K. B. Davis, M.-O. Mewes, M. R. Andrews, N. J. van Druten, D. S. Durfee, D. M. Kurn, and W. Ketterle, Phys. Rev. Lett. **75**, 3969 (1995).

[12] A. Kavokin and B. Gil, Appl. Phys. Lett. **72**, 2880 (1998).

[13] F. Semond, I. R. Sellers, F. Natali, D. Byrne, M. Leroux, J. Massies, N. Ollier, J. Leymarie, P. Disseix, and A. Vasson, Appl. Phys. Lett. **87**, 021102 (2005).

[14] R. Butté, G. Christmann, E. Feltin, J.-F. Carlin, M. Mosca, M. Ilegems, and N. Grandjean, Phys. Rev. B **73**, 033315 (2006).

[15] F. Bernardini, V. Fiorentini, and D. Vanderbilt, Phys. Rev. B **56**, R10024 (1997).

[16] M. Leroux, N. Grandjean, M. Laügt, J. Massies, B. Gil, P. Lefebvre, and P. Bigenwald, Phys. Rev. B **58**, R13371 (1998).

[17] K. Kornitzer, T. Ebner, K. Thonke, R. Sauer, C. Kirchner, V. Schwegler, M. Kamp, M. Leszczynski, I. Grzegory, and S. Porowski, Phys. Rev. B **60**, 1471 (1999).

[18] G. Christmann, R. Butté, E. Feltin, J.-F. Carlin, and N. Grandjean, Phys. Rev. B **73**, 153305 (2006).

[19] E. Feltin, G. Christmann, R. Butté, J.-F. Carlin, M. Mosca, and N. Grandjean, Appl. Phys. Lett. **89**, 071107 (2006).

[20] R. Houdré, R. P. Stanley, and M. Ilegems, Phys. Rev. A **53**, 2711 (1996).

[21] G. Christmann, D. Simeonov, R. Butté, E. Feltin, J.-F. Carlin, M. Mosca, and N. Grandjean, Appl. Phys. Lett. **89**, 261101 (2006).

[22] V. Savona, L. C. Andreani, P. Schwendimann, and A. Quattropani, Solid State Commun. **93**, 733 (1995).

[23] E. Feltin, J.-F. Carlin, J. Dorsaz, G. Christmann, R. Butté, M. Laügt, M. Ilegems, and N. Grandjean, Appl. Phys. Lett. **88**, 051108 (2006).

[24] F. Bernardini and V. Fiorentini, Phys. Status Solidi B **216**, 391 (1999).

[25] M. Leroux, N. Grandjean, J. Massies, B. Gil, P. Lefebvre, and P. Bigenwald, Phys. Rev. B **60**, 1496 (1999).

[26] A. S. Barker, Jr. and M. Ilegems, Phys. Rev. B **7**, 743 (1973).

[27] R. Dingle, A. C. Gossard, and W. Wiegmann, Phys. Rev. Lett. **34**, 1327 (1975).

[28] J. H. Dickerson, E. E. Mendez, A. A. Allerman, S. Manotas, F. Agulló-Rueda, and C. Pecharromán, Phys. Rev. B **64**, 155302 (2001).

[29] Besides, with such a geometry, side QWs (located at an antinode of the cavity light field) would also experience a much different F_{bi} due to the differing nature of the barriers.

[30] V. M. Agranovich, G. C. La Rocca, and F. Bassani, Phys. Status Solidi A **164**, 39 (1997).

[31] G. Panzarini, L. C. Andreani, A. Armitage, D. Baxter, M. S. Skolnick, V. N. Astratov, J. S. Roberts, A. V. Kavokin, M. R. Vladimirova, and M. A. Kaliteevski, Phys. Solid State **41**, 1223 (1999).

[32] M. Smith, J. Y. Lin, H. X. Jiang, and M. Asif Khan, Appl. Phys. Lett. **71**, 635 (1997).

[33] H. A. McLeod, *Thin-Film Optical Filters*, 2nd ed. (Adam Hilger, Bristol, 1986).

[34] R. Butté, E. Feltin, J. Dorsaz, G. Christmann, J.-F. Carlin, N. Grandjean, and M. Ilegems, Jpn. J. Appl. Phys., Part 1 **44**, 7207 (2005).

[35] M. Richard, R. Romestain, R. André, and Le Si Dang, Appl. Phys. Lett. **86**, 071916 (2005).

[36] A weak signature of the UPB is also visible at small angles in the reflectivity spectra (not shown) which is not the case for angle-resolved PL measurements.
[37] D. Brunner, H. Angerer, E. Bustarret, F. Freudenberg, R. Höpler, R. Dimitrov, O. Ambacher, and M. Stutzmann, J. Appl. Phys. **82**, 5090 (1997).
[38] J.-F. Carlin and M. Ilegems, Appl. Phys. Lett. **83**, 668 (2003).
[39] J.-F. Carlin, C. Zellweger, J. Dorsaz, S. Nicolay, G. Christmann, E. Feltin, R. Butté, and N. Grandjean, Phys. Status Solidi B **242**, 2326 (2005).
[40] M. Bayer, T. Gutbrod, A. Forchel, T. L. Reinecke, P. A. Knipp, R. Werner, and J. P. Reithmaier, Phys. Rev. Lett. **83**, 5374 (1999).
[41] Note that the present structure is characterized by a large negative detuning [$\Delta \sim -68$ meV for the case of Fig. 5(b)]. No region with a detuning much closer to zero could be found on this sample owing to its relative uniformity across the wafer.
[42] R. J. Holmes and S. R. Forrest, Phys. Rev. B **71**, 235203 (2005).
[43] Ideally with the uncoupled exciton and cavity modes located on the high energy side of the top dielectric DBR stop band, the best experimental situations would be obtained for Δ values such that $-\Omega_{VRS} \leqslant \Delta \leqslant \Omega_{VRS}$.
[44] The most stringent conditions are fulfilled in absorption experiments since the latter lead to the smallest Ω_{VRS} value [cf. Eq. (20) and Fig. 3 of Ref. 22].
[45] R. P. Leavitt and J. W. Little, Phys. Rev. B **42**, 11774 (1990).
[46] N. Grandjean, B. Damilano, S. Dalmasso, M. Leroux, M. Laügt, and J. Massies, J. Appl. Phys. **86**, 3714 (1999).
[47] R. Butté and N. Grandjean, in *Polarization Effects in Semiconductors: From Ab Initio Theory to Device Applications*, edited by C. Wood and D. Jena (Springer, New York, 2008).
[48] P. Bigenwald, A. Kavokin, B. Gil, and P. Lefebvre, Phys. Rev. B **63**, 035315 (2001).
[49] X.-F. He, Phys. Rev. B **43**, 2063 (1991).
[50] F. Bernardini, V. Fiorentini, and D. Vanderbilt, Phys. Rev. Lett. **79**, 3958 (1997).
[51] S. L. Chuang and C. S. Chang, Phys. Rev. B **54**, 2491 (1996).
[52] S. Schmitt-Rink, D. S. Chemla, and D. A. B. Miller, Phys. Rev. B **32**, 6601 (1985).
[53] Note that the theory of Schmitt-Rink *et al.* (Ref. 52) can be applied to our MQW system as it was developed for QW systems where SL effects do not occur, i.e., a situation where long-range Coulomb interaction effects, known to be weak in quasi-2D systems, between adjacent QWs can be fully neglected.
[54] R. Houdré, J. L. Gibernon, P. Pellandini, R. P. Stanley, U. Oesterle, C. Weisbuch, J. O'Gorman, B. Roycroft, and M. Ilegems, Phys. Rev. B **52**, 7810 (1995).
[55] R. Butté, G. Delalleau, A. I. Tartakovskii, M. S. Skolnick, V. N. Astratov, J. J. Baumberg, G. Malpuech, A. Di Carlo, A. V. Kavokin, and J. S. Roberts, Phys. Rev. B **65**, 205310 (2002).